KAPTON CHARGING CHARACTERISTICS: EFFECTS OF MATERIAL THICKNESS AND ELECTRON-ENERGY DISTRIBUTION

W. S. Williamson, C. R. Dulgeroff, and J. Hymann
Hughes Research Laboratories
Malibu, California 90265

R. Viswanathan
Hughes Space and Communications Group
Los Angeles, California 90009

We report charging characteristics of polyimide (Kapton) of varying thicknesses under irradiation by a very-low-current-density electron beam, with the back surface of the sample grounded. These charging characteristics are in good agreement with a simple analytical model which predicts that in thin samples at low current density, sample surface potential is limited by conduction leakage through the bulk material.

In a second investigation, we measured the charging of Kapton in a low-current-density (3 μAm^{-2}) electron beam in which the beam energy was modulated to simulate Maxwellian and biMaxwellian distribution functions.

INTRODUCTION

The charging characteristics of dielectric thermal-blanket materials in the geosynchronous-earth-orbit (GEO) plasma environment is a subject of considerable importance in spacecraft-charging studies. Polyimide (Kapton) is one of the most commonly used materials in large-area thermal blankets, and this material has been the subject of numerous previous experimental investigations. Many previous studies, however, have employed electron-beam current densities substantially higher than the 3 μAm^{-2} value which we believe represents a reasonable upper bound in the GEO environment.

A second area of concern over ground simulations is that the electron beams that are used are generally monoenergetic, and the charging characteristics that would result in the distributed-energy GEO environment must be inferred from monoenergetic charging data analytically. A model for accomplishing this inference is imbedded in the NASCAP (NASA Charging Analyzer Program) computer code, for example. Since NASCAP is currently being used by spacecraft designers to predict

the spacecraft-charging consequences of their designs, experimental verification of the NASCAP modelling is very timely. A credible distributed-energy electron source is needed to perform these experiments, and we describe a simple means for devising such a source below.

SYMBOLS USED

I_B	electron-beam current density (no sample in place)
I_P	electron-beam current density (incident on charged sample)
ε_R	Electron reflux coefficient (including backscatter + secondaries)
σ	bulk conductivity of sample
A	sample area
d	sample thickness
V_S	sample surface potential
eV_B	electron-beam energy
I_R	current of refluxed electrons ($=\varepsilon_R I_P$)
k	$=dJ_B\sigma^{-1}$
J_B	electron beam current density
$f_I(V_B)$	electron-current distribution function

Only SI units are used in this paper.

KAPTON CHARGING CHARACTERISTICS IN MONOENERGETIC ELECTRON BEAMS

In this section we describe the experimental apparatus and measurements and then present a simple analytical model for comparison with the experimental results.

Experimental Apparatus and Measurements

The experiments were conducted in a 0.6-m-diameter vacuum chamber, which is shown in Figure 1. A divergent-beam electron flood gun, shown in Figure 2, is used to irradiate the sample. This electron gun is built to a design developed at NASA Lewis Research Center. It produces a broad uniform-current-density beam and exhibits excellent stability over a wide range of current densities. The sample is housed in a separate antechamber which can be isolated from the main chamber by a vacuum gate valve. The geometry of the sample and sample holder is shown in Figure 3.

We have measured the charging characteristics of Kapton under conditions which differ significantly from previous practice: we employed an electron-beam current density of 3 μAm^{-2}, and we mounted the sample by wrapping it around the edges of the metal sample-holder and clamping it at the rear. These two innovations are more representative of the electron current

density which exists at GEO, and of the geometry with which thermal-blanket materials are exposed to electron bombardment on GEO spacecraft. We exposed Kapton samples of two thicknesses (25 μm and 127 μm) to irradiation by monoenergetic electron beams with energies up to 14 keV. A typical charging characteristic is shown in Figure 4, where the surface potential of 127-μm-thick Kapton is shown as a function of time, during continuous bombardment by 14-keV electrons. This plot reveals the relatively long time constant involved in charging at these low current densities.

Figure 5 shows the equilibrium surface potential of 127-μm-thick Kapton as a function of incident beam-current energy from 2 keV to 14 keV. The straight-line characteristic intercepts the beam-energy axis at an energy of about 1.6 keV; this energy corresponds to the "second-crossing" energy, i.e., the energy at which the secondary-electron yield of the material is unity. Figure 6 shows the corresponding characteristic of 25-μm-thick Kapton, under the same test conditions. In this curve, the second-crossing intercept is the same, but the surface potential saturates at much lower values than were observed in the 127-μm-thick material. This saturation effect is produced by conduction losses through the bulk Kapton, as evidenced by the fact that the saturation effect disappears when the ground connection on the rear of the sample is removed; the characteristic then remains linear within the limits of our beam-energy capability. We have developed a simple analytical model which successfully predicts the surface potential at which the saturation effect occurs. This model is similar to previous models due to Purvis, et. al. (Reference 1) and Reeves and Balmain (Reference 2), except that it conforms to the specific geometry of the test environment that we used. This model predicts that the saturation surface potential of Kapton depends on the parameter $k=dJ\sigma^{-1}$, where d is the sample thickness, J is the electron-beam current density, and σ is the material conductivity. Material testing with thick (large-d) samples and high current densities (large J) raise the saturation potential beyond usual test limits. This explains why the saturation effect shown in Figure 6 is not often seen in published dielectric-charging results; the saturation is produced by the use of thinner materials and lower electron-beam current densities than are commonly used in material-charging tests.

Analytical Charging Model

In this section we present the simple model of sample charging which we will evaluate by comparison with experimental data. This model is highly simplified and applies to an equilibrium-charge condition (i.e., a condition in which displacement currents and stored charge can be neglected). It also assumes that cylindrical Langmuir-probe theory correctly calculates the reduction in current that is collected by the sample as it charges more and more negative.

In equilibrium, the current that is incident on a charged sample is given by

$$I_P = I_R + \frac{\sigma A}{d} V_S \qquad (1)$$

where the first term corresponds to refluxed electrons that are ejected from the surface by backscatter or secondary-electron emission, and the second term corresponds to conduction loss of electrons through the sample to the grounded rear surface. According to cylindrical Langmuir probe theory (Reference 3), the current that is collected by a charged sample is related to the incident current (i.e., current that would be collected by an uncharged sample) by

$$I_P = I_B \frac{V_B - V_S}{V_B} \qquad (2)$$

The foregoing expressions can be combined to yield the surface voltage as a function of beam voltage:

$$V_S = \frac{V_B k(1-\epsilon_R)}{V_B + k(1-\epsilon_R)} \qquad (3)$$

Of course, the reflux coefficient ϵ_R is a function of the impact energy of electrons which strike the surface, $e(V_B - V_S)$; this function, along with the constants contained within k, are in general known only numerically. Equation (3) does not represent a solution for V_S; it can, however, be solved for V_S numerically by a simple iterative procedure.

We have solved Equation (3) numerically, using the Kapton reflux-coefficient and conductivity data that is contained within NASCAP, and values of material thickness and beam current density that are appropriate to our experimental conditions. The results are shown in Figure 7, where we compare the actual equilibrium charging voltages with the values predicted by the model, for several thicknesses of Kapton. The model predictions provide reasonably accurate descriptions of the shape of the charging characteristics and the location of the beam energy at which conduction-induced saturation of the charging voltage begins.

Figure 8 shows the solutions to Equation (3) plotted in a different manner: here the parameter k is used as the independent variable, and electron-beam energy is a parameter. Notice that the curves are spaced evenly in surface voltage V_S for large values of k (i.e., large current density and/or low conductance), and that the surface potential is independent of k in this

region. This case corresponds to the situation in which the impacting electron current is balanced totally by electron reflux. For low values of k, conduction losses become significant, causing the curves to pack together at higher values of V_B. Figure 8 is a convenient tool for estimating Kapton charging; it could be easily reproduced for other dielectrics for which ϵ_R is known by solving Equation (3).

KAPTON CHARGING UNDER DISTRIBUTED-ENERGY ELECTRON-BEAM IRRADIATION

As described in the Introduction, realistic simulation of spacecraft charging should include the use of a distributed-energy electron source. In principle, of course, multiple experiments can be performed using monoenergetic beams and calculating the expected surface potential using a model such as that given above. This calculation entails solving Equation (3) as before, but using an effective reflux coefficient such as

$$\langle \epsilon_R \rangle (V_S) = \int_{V_S}^{\infty} \epsilon_R (V_B - V_S) f_I (V_B) \, dV_B \qquad (4)$$

instead of the monoenergetic ϵ_R used above. This approach is hazardous because the effective ϵ_R may differ from that given by Equation (4); that is, the electron reflux which results from the simultaneous presence of two electron-energy species may differ from the sum of the refluxes that would result from each energy species being separately present. Such nonlinearities are well known in the case of sputtering of solids by ion bombardment, but we are unaware of electron-reflux data which would either validate Equation (4) or provide a useful alternative.

In order to provide an empirical foundation for these distributed-energy electron distribution considerations, we have developed a simple and novel means of simulating the broad distribution of electron energies which simultaneously bombard a spacecraft in GEO. We have used this tool to study the charging of 25-μm- and 127- μm-thick Kapton. We find that the thinner material, which is in the conduction-dominated (saturated surface-potential) regime charges to essentially the same surface potential regardless of the electron distribution function. The thicker material, however, experiences more severe charging when exposed to electrons which are distributed in energy corresponding to "moderate" and "severe" charging conditions than it does when exposed to a "quiescent" distribution of electron energies.

Figure 9 illustrates the arrangement of our distributed-energy electron source. The electron source, shown in Figure 2, is a simple hot-cathode source with multiple wire-mesh grids to extract a broad, spatially uniform electron beam. The

e-gun is powered by a programmable high-voltage power supply which operates over the range of 0 to 30 kV. The power supply is programmed by a microcomputer; the microcomputer causes the power supply to generate a repetitive sequence of electron-beam voltages. This repetitive sequence, which is defined in the microcomputer firmware is arranged in such a manner that the time-averaged current produced by the e-gun at a given energy is equal to that which exists in the GEO environment. That is, the system selects an electron-beam energy and causes the power supply to output the corresponding voltage for a time duration that is proportional to the value of the desired current distribution function at that energy. The energies are output in an ascending-energy sequence, but we have found that the same sample charging is produced for descending- or random-energy sequences.

This simulation is reasonable if the time scale within which the electron-beam energy is varied is short compared to the sample charging time. This condition is satisfied in our tests, because the electron-beam energy is varied over a 5-s time period, while the sample typically requires an hour or more to reach equilibrium potential (in cases in which the sample is not grounded at the rear surface, equilibration still requires several minutes). The microcomputer is programmed to generate any of three electron-energy distribution functions (which it selects by reading the position of a front-panel switch); the programs are written in a commercially available integer BASIC and are stored in ROM for convenience.

The three distribution functions we use are a biMaxwellian distribution characteristic of quiescent conditions (Reference 4) and two single-Maxwellian distributions recommended by Stevens (Reference 5) to simulate the moderate and solar-substorm GEO environments. The three distribution functions have identical total currents. These distributions are plotted in Figure 10.

Figure 11 shows the response of both 25-μm- and 127-μm-thick Kapton under irradiation by the multienergetic-beam apparatus. The thicker Kapton charges to substantially higher voltages and evidences a larger difference between the three distribution functions than does the thinner material. It is clear that the single-Maxwellian distribution that simulates "moderate" charging conditions is significantly more severe than the biMaxwellian "quiescent" condition.

REFERENCES

1. C.K. Purvis, N.J. Stevens, and J.C. Oglebay, "Charging Characteristics of Materials: Comparison of Experimental Results with Simple Analytical Models," procedings of the Spacecraft Charging Technology Conference, AFGL-TR-77-0051, NASA TMX-73537, p. 459 (1977).

2. R.D. Reeves and K.G. Balmain, "Two-Dimensional Electron Beam Charging Model for Polymer Films," IEEE Trans. on Nuc. Sci. NS-28, 4547 (1981).

3. F.F. Chen, "Electric Probes," Pure and Applied Physics 21, Plasma Diagnostic Techniques, eds. R. H. Huddlestone and S.L. Leonard. Academic Press, 1965, pp 113-119.

4. H.B. Garrett and S. E. DeForrest, " An Analytical Simulation of the Geosynchronous Plasma Environment," Planet. Space Sci. 27, 1101 (1979).

5. N.J. Stevens, "Design Practices for Controlling Spacecraft Charging Interactions," AIAA Paper No. 82-0115, presented at the AIAA 20th Aerospace Sciences Conference, Orlando, Florida, 11-14 January 1982.

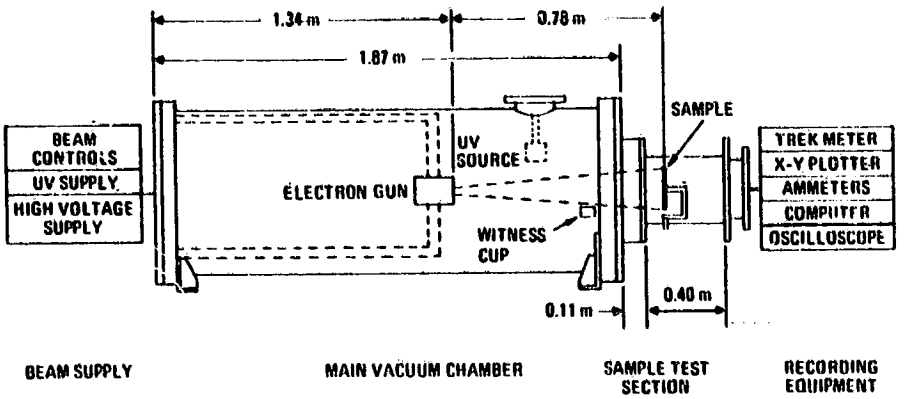

Figure 1. - Hughes spacecraft-charging-simulation facility: overview.

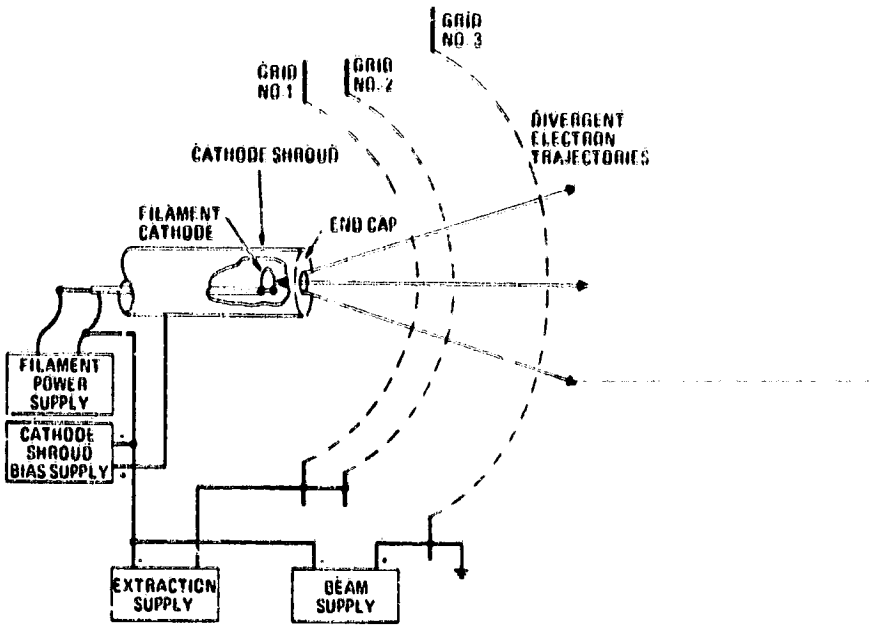

Figure 2. - Electron source (NASA Lewis design).

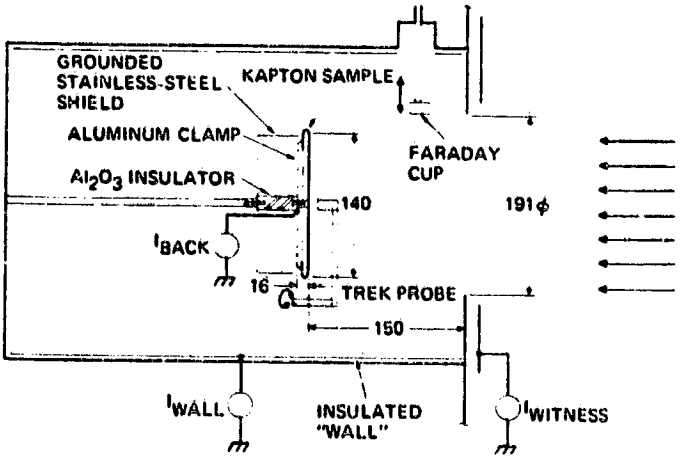

Figure 3. - Hughes spacecraft-charging-simulation facility: sample test section details. Dimensions are in millimeters.

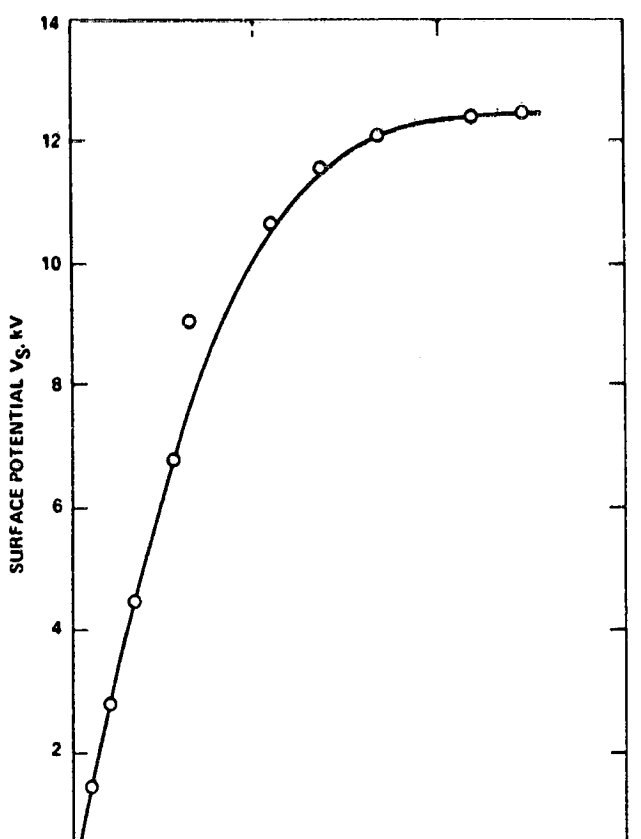

Figure 4. - Surface potential of 127-μm-thick Kapton under irradiation by a 14-keV, 3-μAm^{-2} electron beam.

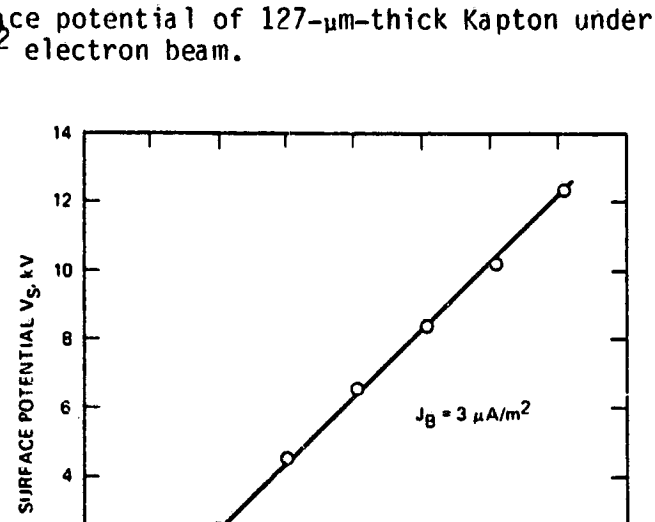

Figure 5. - Equilibrium surface potential of 127-μm-thick Kapton as a function of electron beam energy.

C-7

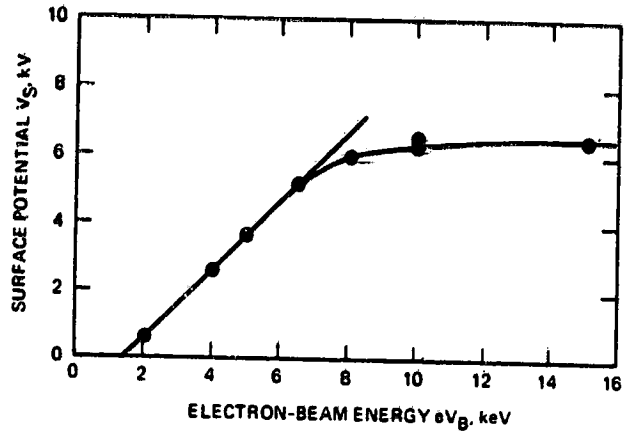

Figure 6. - Surface potential of 25-μm-thick Kapton.

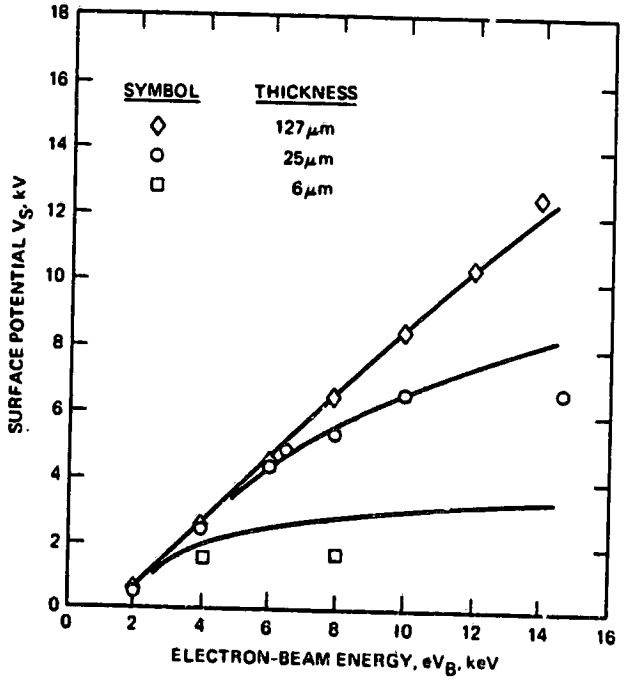

Figure 7. - Comparison of predictions of analytical model with experimental results for charging of Kapton of several thicknesses.

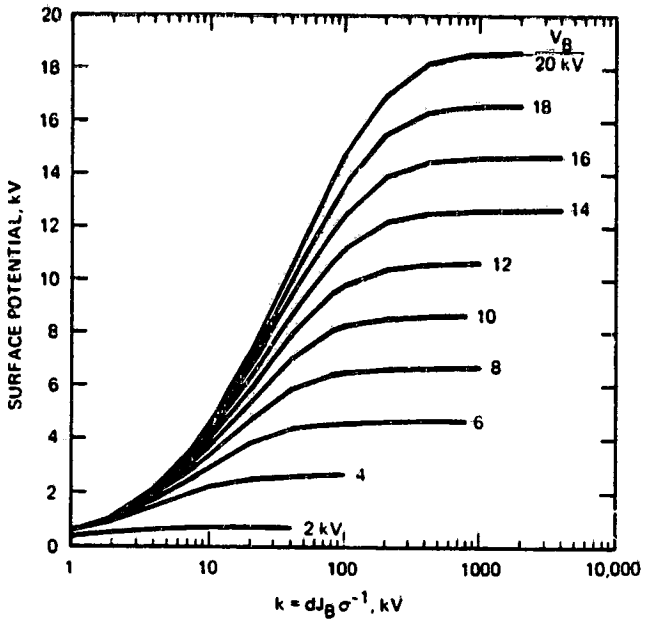

Figure 8.- Analytical charging model for Kapton, showing surface potential as a function of $k = dJ_B\sigma^{-1}$, with beam voltage V_B as a parameter.

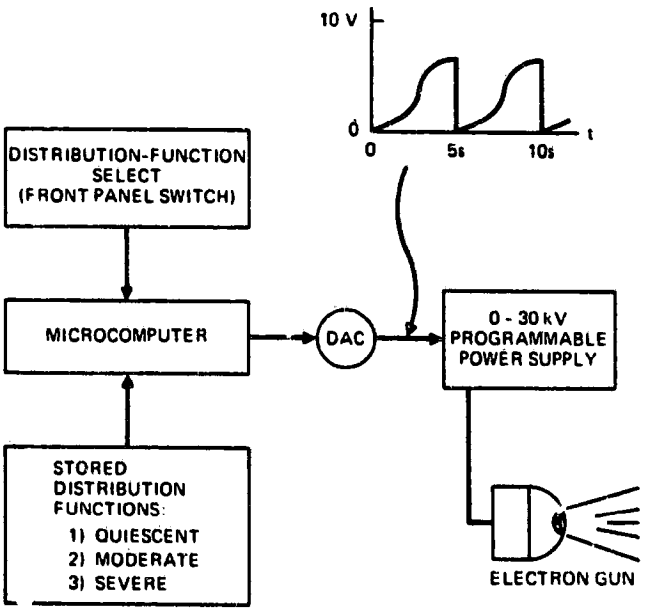

Figure 9. - Block diagram of multienergetic electron beam.

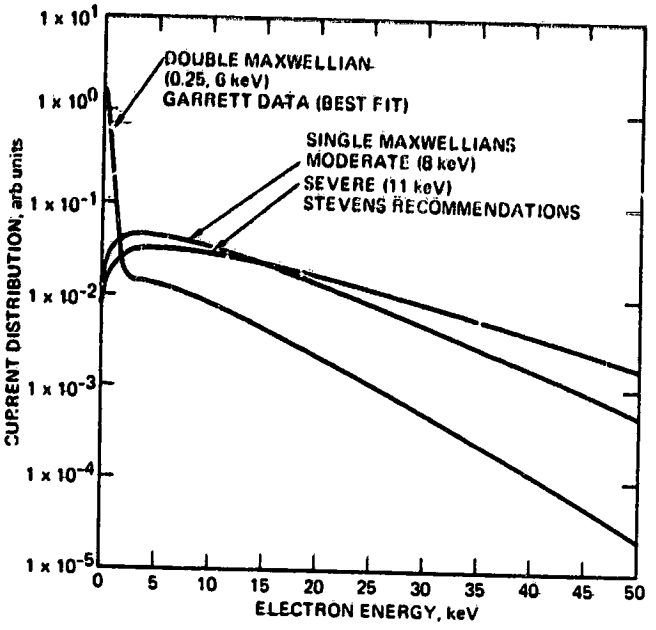

Figure 10. - Electron energy distribution for simulation experiments.

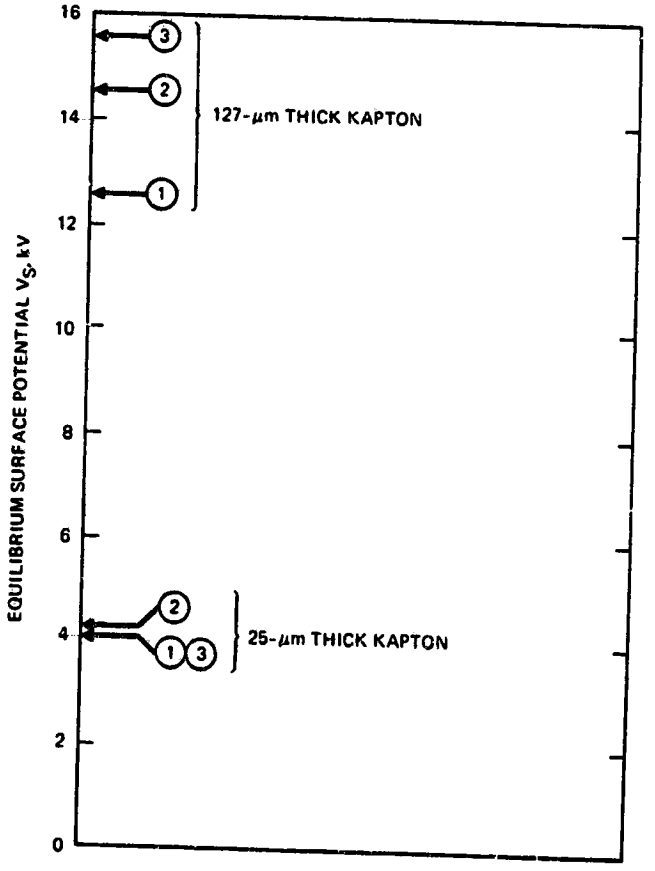

Figure 11. - Equilibrium surface potential of 25- and 127-μm-thick Kapton irradiated by 3-μAm^{-2} multienergetic electron beam: (1) = "quiescent", (2) = "moderate", (3) = "severe" charging environments.